arXiv:2302.00512v1 [physics.plasm-ph] 1 Feb 2023

Decay law of magnetic turbulence with helicity balanced by chiral fermions

Axel Brandenburg,[1,2,3,4] Kohei Kamada,[5] and Jennifer Schober[6]

[1]*Nordita, KTH Royal Institute of Technology and Stockholm University, 10691 Stockholm, Sweden*
[2]*The Oskar Klein Centre, Department of Astronomy, Stockholm University, AlbaNova, SE-10691 Stockholm, Sweden*
[3]*School of Natural Sciences and Medicine, Ilia State University, 0194 Tbilisi, Georgia*
[4]*McWilliams Center for Cosmology and Department of Physics, Carnegie Mellon University, Pittsburgh, Pennsylvania 15213, USA*
[5]*Research Center for the Early Universe (RESCEU), Graduate School of Science, The University of Tokyo, Hongo 7-3-1, Bunkyo-ku, Tokyo 113-0033, Japan*
[6]*Laboratoire d'Astrophysique, EPFL, CH-1290 Sauverny, Switzerland*

(Dated: February 2, 2023)

In relativistic plasmas of sufficiently high temperature, fermion chirality can be interchanged with magnetic helicity while preserving the total chirality through the quantum chiral anomaly. Here we show, using a high resolution numerical simulation, that in the case of zero total chirality, where the magnetic helicity density balances with the appropriately scaled chiral chemical potential to zero, the magnetic energy density decays and the correlation length increases with time just like in nonhelical turbulence with vanishing chiral chemical potential. But here, the magnetic helicity density is nearly maximum and shows a novel scaling with time t proportional to $t^{-2/3}$. This is unrelated to the $t^{-2/3}$ decay of magnetic *energy* in fully helical magnetic turbulence. The modulus of the chiral chemical potential decays in the same fashion. These decay laws can be determined from the conservation of what is known as the Hosking integral, adapted here to include the effect of the chiral chemical potential. We compute the adapted Hosking integral and confirm that it is indeed approximately conserved.

Magnetic helicity characterizes the knottedness of magnetic field lines and plays important roles in cosmological, astrophysical, and laboratory plasmas. Since the early work of Woltjer of 1958 [1], we know that the magnetic helicity is an invariant of the ideal magnetohydrodynamic (MHD) equations. Even in the non-ideal case of finite conductivity, it is asymptotically conserved in the limit of large magnetic Reynolds numbers [2]. This is because, unlike the magnetic energy dissipation, which is finite at large magnetic Reynolds numbers, the magnetic helicity dissipation converges to zero in that limit [3]. The magnetic helicity controls the decay of magnetic fields in closed or periodic domains, provided the magnetic helicity is finite. However, even when the net magnetic helicity over the whole volume vanishes, there can still be random fluctuations of magnetic helicity. Also in this case, the conservation of magnetic helicity still plays an important role in smaller subvolumes, as was only shown recently [4]. The conserved quantity in that case is what is now known as the Hosking integral [5, 6], which characterizes magnetic helicity fluctuations in smaller subvolumes [4].

At relativistic energies, the chirality of fermions combines with the helicity of the magnetic field to a total chirality that is *strictly* conserved in a periodic or closed domain – even for finite magnetic diffusivity [7, 8] which is a consequence of the chiral anomaly [9, 10]. This can have a number of consequences. There is an instability that can amplify a helical magnetic field [11]. It is now often referred to as the chiral plasma instability [12] and it causes the chiral chemical potential carrying the chirality of the fermions to decay such that the total chirality remains unchanged [13–15]. Conversely, if a helical magnetic field decays, the chiral chemical potential can increase [16, 17]. Finally, when the chiral chemical potential balances the magnetic helicity to produce vanishing total chirality of the system, which is realized, e.g., in cosmological MHD after axion inflation [18–20], the magnetic field can only decay. One may wonder whether the decay is triggered by the chiral plasma instability and is hence exponential [18, 19]. However, it turns out that this decay occurs in a power-law fashion that is similar to the MHD decay of magnetic fields in the absence of magnetic helicity [21], which is governed by the conservation of the Hosking integral. The purpose of this Letter is to study whether the decay of the magnetic field in chiral MHD is also governed by a correspondingly adapted Hosking integral. While the model adopted here is based on quantum electrodynamics, the extension to the realistic cosmological models based on the Standard Model of particle physics is straightforward; see, e.g., Ref. [14, 22].

The Hosking integral $I_{\rm H}$ is defined as the asymptotic limit of the relevant magnetic helicity density correlation integral, $\mathcal{I}_{\rm H}(R)$, for scales R large compared to the correlation length of the turbulence, $\xi_{\rm M}$, but small compared to the system size L. The function $\mathcal{I}_{\rm H}(R)$ is given by

$$\mathcal{I}_{\rm H}(R)=\int_{V_R}\langle h(\boldsymbol{x})h(\boldsymbol{x}+\boldsymbol{r})\rangle\,{\rm d}^3r, \tag{1}$$

where V_R is the volume of a ball of radius R and, in MHD, $h = \boldsymbol{A}\cdot\boldsymbol{B}$ is the magnetic helicity density with $\boldsymbol{A}$ being the magnetic vector potential, so $\boldsymbol{B} = \boldsymbol{\nabla}\times\boldsymbol{A}$. Here, angle brackets denote averages over the volume L^3.

For relativistic chiral plasmas, on the other hand, we now amend the magnetic helicity density with a contribution from the chiral chemical potential μ_5. We work here with the scaled chiral chemical potential $\mu_5 \to \mu_5' = (4\alpha/\hbar c)\,\mu_5$, where α is the fine structure constant, $\hbar$ is the reduced Planck constant, and c is the speed of light. Our rescaled μ_5' has the dimension of a wave number. From now on, we drop the prime and only work with the rescaled chiral chemical potential. We also define the quantity $\lambda = 3\hbar c\,(8\alpha/k_{\rm B}T)^2$, where $k_{\rm B}$ is the Boltzmann constant and T is the temperature. We define the total helicity density $h_{\rm tot} \equiv \boldsymbol{A}\cdot\boldsymbol{B} + 2\mu_5/\lambda$ and replace $h \to h_{\rm tot}$ when defining the adapted Hosking integral.

Similarly to earlier studies of non-relativistic chiral plasmas ($\mu_5 \to 0$) with a helical magnetic field, the case of a finite net chirality, $\langle h_{\rm tot}\rangle \neq 0$, is governed by the conservation law for $\langle h_{\rm tot}\rangle$. Of course, when $\langle h_{\rm tot}\rangle = 0$, it is still conserved, but it can then no longer determine the dynamics of the system. This is when we expect, instead, I_H to control the dynamics of the decay. In the following, we focus on this case using numerical simulations to compute the decay properties of a turbulent magnetic field and the conservation properties of I_H using the total helicity in a relativistic plasma.

In the presence of a finite chiral chemical potential, the evolution equations for $\boldsymbol{A}$ and μ_5 are [8]

$$\frac{\partial\boldsymbol{A}}{\partial t} = \eta(\mu_5\boldsymbol{B} - \boldsymbol{J}) + \boldsymbol{u}\times\boldsymbol{B}, \quad \boldsymbol{J} = \boldsymbol{\nabla}\times\boldsymbol{B}, \tag{2}$$

$$\frac{\partial\mu_5}{\partial t} = -\frac{2}{\lambda}\eta(\mu_5\boldsymbol{B} - \boldsymbol{J})\cdot\boldsymbol{B} - \boldsymbol{\nabla}\cdot(\mu_5\boldsymbol{u}) + D_5\nabla^2\mu_5, \tag{3}$$

where η is the magnetic diffusivity, D_5 is the diffusion coefficient of μ_5, spin flipping is here neglected (but see [21] for cases where it is not), and $\boldsymbol{u}$ is the velocity, which is governed by the compressible Navier-Stokes equations [8, 23, 24]

$$\frac{{\rm D}\boldsymbol{u}}{{\rm D}t} = \frac{2}{\rho}\boldsymbol{\nabla}\cdot(\rho\nu\mathsf{S}) - \frac{1}{4}\boldsymbol{\nabla}\ln\rho + \frac{\boldsymbol{u}}{3}(\boldsymbol{\nabla}\cdot\boldsymbol{u} + \boldsymbol{u}\cdot\boldsymbol{\nabla}\ln\rho) - \frac{\boldsymbol{u}}{\rho}\left[\boldsymbol{u}\cdot(\boldsymbol{J}\times\boldsymbol{B}) + \eta\boldsymbol{J}^2\right] + \frac{3}{4\rho}\boldsymbol{J}\times\boldsymbol{B}, \tag{4}$$

$$\frac{\partial\ln\rho}{\partial t} = -\frac{4}{3}(\boldsymbol{\nabla}\cdot\boldsymbol{u} + \boldsymbol{u}\cdot\boldsymbol{\nabla}\ln\rho) + \frac{1}{\rho}\left[\boldsymbol{u}\cdot(\boldsymbol{J}\times\boldsymbol{B}) + \eta\boldsymbol{J}^2\right],$$

where $\mathsf{S}_{ij} = (\partial_i u_j + \partial_j u_i)/2 - \delta_{ij}\boldsymbol{\nabla}\cdot\boldsymbol{u}/3$ are the components of the rate-of-strain tensor, ν is the kinematic viscosity, ρ is the density (which includes the rest mass density), and the ultrarelativistic equation of state for the pressure $p = \rho/3$ has been employed.

In the following, we assume uniform ν, η, and D_5 such that $\nu = \eta = D_5$. By setting $c = 1$ and $k_0 = 1$, we fix the units of velocity and length. The unit of time is then automatically $(ck_0)^{-1}$. We set initially $\rho = \rho_0 = 1$, which then also fixes the units of energy. Our use of Eq. (4) compared to the nonrelativistic counterpart only affects the kinetic energy and not the magnetic field evolution; see Ref. [25] for comparisons in another context.

In the following, we make use of spectra that are defined as the squared modulus of the Fourier transformed quantity, integrated over concentric shells in wave number space. An example is ${\rm Sp}(\boldsymbol{B})$, which is a function of $k \equiv |\boldsymbol{k}|$ and t, normalized such that $\int {\rm Sp}(\boldsymbol{B})\,{\rm d}k = \langle\boldsymbol{B}^2\rangle$ [24]. We define the mean magnetic energy density $\mathcal{E}_{\rm M} = \langle\boldsymbol{B}^2\rangle/2$ and the mean magnetic helicity density $\mathcal{H}_{\rm M} = \langle\boldsymbol{A}\cdot\boldsymbol{B}\rangle$, as well as the correlation length of the magnetic field, $\xi_{\rm M} = \mathcal{E}_{\rm M}^{-1}\int k^{-1}E_{\rm M}\,{\rm d}k$ with $E_{\rm M}(k,t) \equiv {\rm Sp}(\boldsymbol{B})/2$. The magnetic helicity spectrum $H_{\rm M}(k,t)$ is defined such that $\int H_{\rm M}\,{\rm d}k = \mathcal{H}_{\rm M}$.

For an initially uniform $\mu_5 \equiv \mu_{50}$, Eq. (2) has exponentially growing solutions proportional to $e^{{\rm i}\boldsymbol{k}\cdot\boldsymbol{x}+\gamma_5 t}$, when $k < \mu_5$. The maximum growth rate is $\gamma_5 = \mu_5^2\eta/4$ for $k = k_5 = \mu_5/2$ [8, 23]. As initial condition for $\boldsymbol{A}$, we consider a Gaussian distributed random field with a magnetic energy spectrum that is a broken power law with $E_{\rm M}(k,t) \propto k^4$ for $k < k_0$, motivated by causality constraints [26], and a Kolmogorov-type spectrum, $E_{\rm M}(k,t) \propto k^{-5/3}$, for $k > k_0$, which may be expected of there is a turbulent forward cascade.

We solve the governing equations using the Pencil Code [27], where the equations are already implemented [28, 29]. We consider a cubic domain of size L^3, so the smallest wave number is $k_1 = 2\pi/L$. The largest wave number is $k_{\rm Ny} = k_1 N/2$, where N is the number of mesh points in one direction. In choosing our parameters, it is important to observe that $k_1 \ll k_0 \ll k_5 \ll k_{\rm Ny}$. Here, we choose $k_1 = 0.02$, $k_0 = 1$, $k_5 = 5$, and $k_{\rm Ny} = 10.24$, using $N = 1024$ mesh points in each of the three directions. This means that $|\mu_{50}| = 10$, which is virtually the same as $k_{\rm Ny}$. However, experiments with other choices, keeping $N = 1024$, showed that ours yields an acceptable compromise that still allows us to keep k_1 small enough. We choose the sign of μ_5 to be negative, and adjust the amplitude of the magnetic field such that $2\mathcal{E}_{\rm M}\xi_{\rm M} = \mathcal{H}_{\rm M} = -2\mu_{50}/\lambda$. Using $\eta = 2\times10^{-4}$ and $\lambda = 2\times10^4$, we have, following Ref. [25], $v_\lambda \equiv \mu/\sqrt{\rho\lambda} \approx 0.07$ and $v_\mu \equiv \mu\eta = 0.002$, so $v_\lambda/v_\mu \approx 35 \gg 1$, corresponding to what is called regime I.

In Figure 1(a), we present magnetic energy spectra at different times. We clearly see an inverse cascade where the spectral magnetic energy increases with time for $k \ll k_0$ (indicated by the upward arrow), but decays for $k \gg k_0$. As time goes on, the peak of the spectrum moves to smaller wave numbers with $k_{\rm peak} \approx \xi_{\rm M}^{-1}$, where $\xi_{\rm M}$ increases approximately like a power law, $\xi_{\rm M} \propto t^q$, while the energy density decreases, also approximately like a power law with $\mathcal{E}_{\rm M} \propto t^{-p}$. The spectral peak always evolves underneath an envelope $\propto k^{3/2}$, which implies that $\max[E_{\rm M}(k,t)] = \xi_{\rm M}(t)^{-\beta}$ with $\beta = 3/2$, indicated

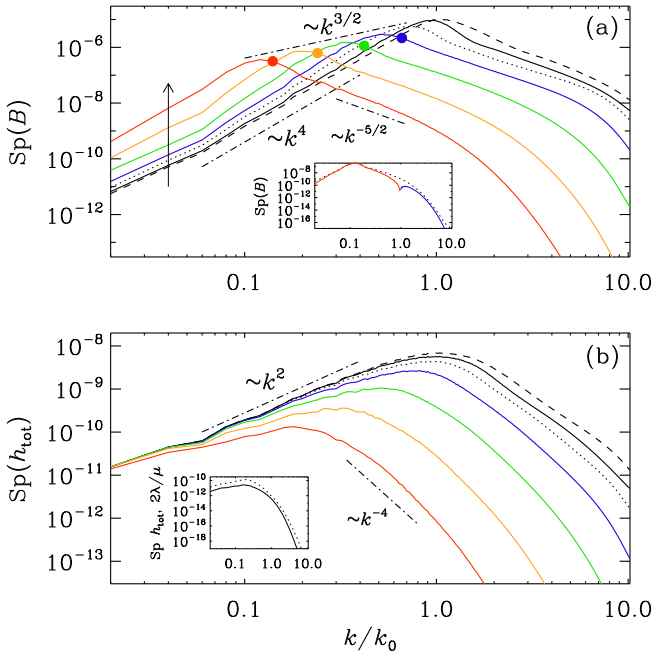


FIG. 1. (a) Magnetic energy and (b) total helicity variance spectra at $t = 31$ (dashed), 100 (solid), 316 (dotted), 10^3 (blue), 3.16×10^3 (green), 10^4 (orange), and 3.16×10^4 (red). In (a), note that Sp($\boldsymbol{B}^2$) evolves underneath the envelope $k^{3/2}$, and the upward arrow indicates the sense of time. For orientation, the slopes $k^{-5/2}$ and k^{-4} have been indicated in what is expected to correspond to the inertial ranges in (a) and (b), respectively. In (a), the inset shows $(k/2)\,H_{\rm M}(k)$ at the last time with positive (negative) values in red (blue), and in (b), the inset compares Sp($2\mu_5/\lambda$) (solid) with Sp($h_{\rm tot}$) (dotted) at the last time.

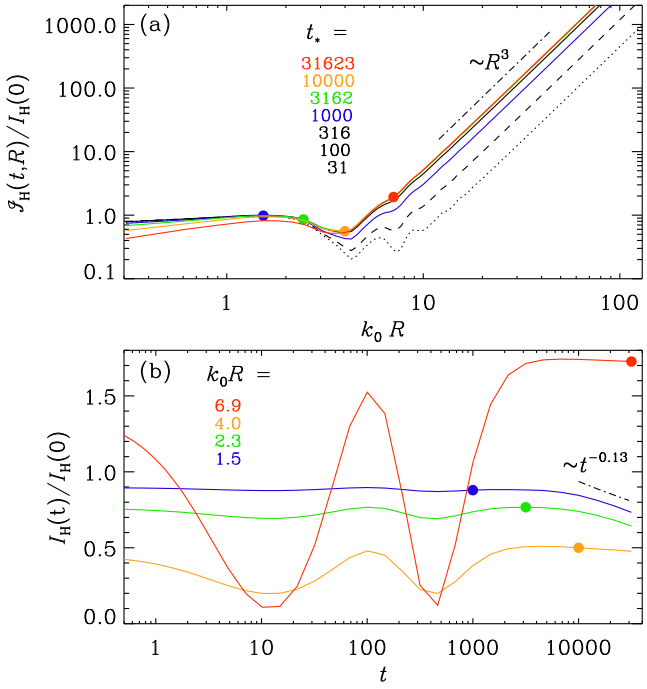


FIG. 2. (a) $\mathcal{I}_H(R,t)$ versus R for different times t_* (indicated by the same colors/line styles as in Figure 1), and (b) $\mathcal{I}_H(R,t)$ versus t (normalized) for $R=\xi_{\rm M}(t_*)$ marked by the four colors. The $t^{-0.13}$ scaling is indicated as the dashed-dotted curve for comparison. In (a), the four colored symbols indicate the positions of $k_0\xi_{\rm M}(t_*)$, and in (b), the time dependencies are plotted for those $R=\xi_{\rm M}(t_*)$.

by the upper dashed-dotted line in Figure 1(a).

To compute $\mathcal{I}_{\rm H}$ (and thereby $I_{\rm H}$), we employ a spectral technique by computing the total helicity variance spectrum Sp($h_{\rm tot}$); see Figure 1(b). Compared to the inverse cascade seen in Sp($\boldsymbol{B}$), we here see the conservation of the large-scale total helicity variance spectrum $\propto k^2$. We thus obtain

$$\mathcal{I}_H(R,t) = L^{-3}\int w(\boldsymbol{k},R)\,{\rm Sp}(h_{\rm tot})\,{\rm d}^3\boldsymbol{k}/(2\pi)^3. \quad (5)$$

Here, we choose $w(k,R) = (4\pi R^3/3)[6j_1(kR)/kR]^2$ as weight function [6] with j_n being spherical Bessel functions.

In Figure 2(a) we plot $\mathcal{I}_H(R,t)$ versus R for different values of t, and in Figure 2(b) versus t for four choices of R, indicated by the colored lines in both panels. It turns out that $\mathcal{I}_H(R)$ is nearly flat for $k_0R \ll 10$, but grows cubically for $k_0R \gg 1$. This is different for non-helical MHD with non-chiral plasmas [4, 6], where $\mathcal{I}_H(R)$ was found to grow cubically for small R and is flat for large R, i.e., just the other way around. Cubic scaling of $\mathcal{I}_H(R)$ implies that the total helicity density in subvolumes is space filling and does not change randomly. At small R, scaling is spatially flat. This is also where Sp($2\mu_5/\lambda$) has a large contribution (in addition to that at $k=0$). This suggests that here the total magnetic helicity is spatially random. This is consistent with the finding that the magnetic energy produced by the chiral plasma instability is rather weak [30]. Note also that the transition to cubic scaling happens only for $R > \xi_{\rm M}$, which might explain why the Hosking integral determines the decay until the end of the simulation.

As a function of time, we see that for $k_0R \approx 4$ (orange) and 7 (red), $\mathcal{I}_H(R,t)$ shows large excursions, but no net trend; see Figure 2(b). These excursions are caused by the oscillatory nature of the weight function in Eq. (5) [30]. It should also be noted that the time axis is on a logarithmic scale, so the excursions are still at comparatively early times. For $k_0R = 1.5$ (blue), $\mathcal{I}_H(R,t)$ is nearly constant, which suggests the conservation of the adapted Hosking integral, but we see a decline at late times. In spite of the semilogarithmic representation, we can see that this decline corresponds to a $t^{-0.13}$ scaling, which is weak and similar to what has been seen for other simulations at that resolution; see, e.g., Ref. [31]. While our choice of the relevant value of R is not well

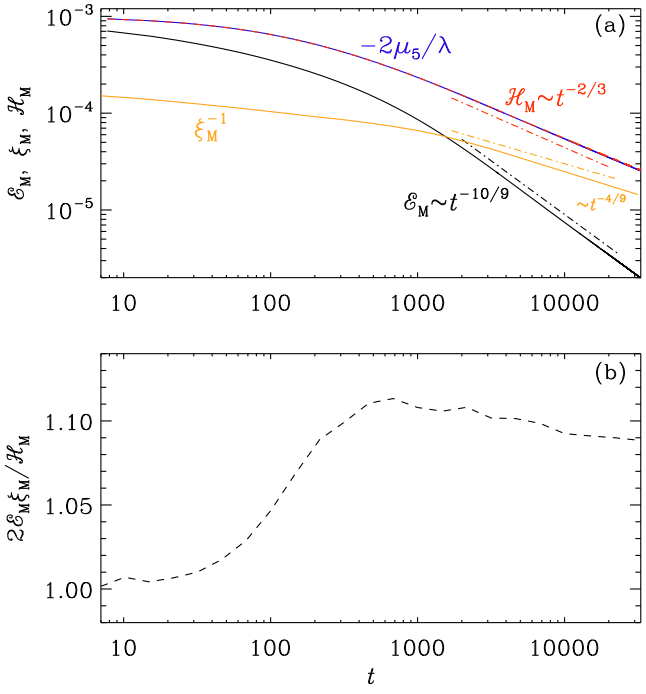


FIG. 3. Time dependence of (a) $\mathcal{E}_M$ (black), ξ_M (orange), $\mathcal{H}_M$ (blue), and $-2\mu_5/\lambda$ (red), and (b) $2\mathcal{E}_M\xi_M/\mathcal{H}_M$.

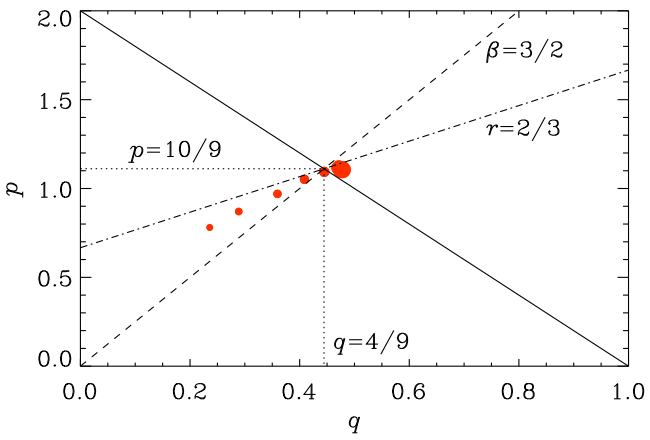


FIG. 4. pq diagram for times t = 700, 1000, 1500, 2200, 3200, 4600, 6800, 10^4, 1.5×10^4, 1.5×10^4, 2.2×10^4, and 3.2×10^4, corresponding to symbols of increasing size. The solid line denotes the scale-invariance line $p=2(1-q)$, the dashed line the $\beta=3/2$ line for adapted Hosking scaling, and the dashed-dotted line is the new $r=2/3$ line that does not have any correspondence in standard MHD.

determined, we present in the following a different argument of why the adapted Hosking integral is actually conserved.

As in the case of nonrelativistic MHD ($\mu_5\to0$), the dimensions of $\mathcal{I}_H$ and I_H are $\mathrm{cm}^9\,\mathrm{s}^{-4}$. This implies that in $\xi_M\propto t^q$, the value of the exponent is $q=4/9$, if the conservation of $\mathcal{I}_H$ determines the time evolution of the magnetic field around the characteristic scale. Next, assuming selfsimilarity, the magnetic spectra can be collapsed on top of each other by plotting them versus $k\xi_M(t)$ and compensating the decline in the height by ξ_M^β to yield the universal function $\phi(k\xi_M)=\xi_M^\beta E_M(k\xi_M)$; see Appendix B of Ref. [6] and Refs. [31, 32] for examples in other contexts. Using also the invariance of the spectrum under rescaling [33], $\boldsymbol{x}\to\boldsymbol{x}'=\boldsymbol{x}\ell$ and $t\to t'=t\ell^{1/q}$, and since the dimension of $E_M(k,t)$ is $\mathrm{cm}^3\,\mathrm{s}^{-2}$, we have $E_M(k\ell^{-1},t\ell^{1/q})=\ell^{3-2/q+\beta}[\xi_M\ell]^{-\beta}\phi(k\xi_M)$, and therefore $\beta=2/q-3=3/2$, which agrees with Figure 1(a). Finally, for $\mathcal{E}_M\propto t^{-p}$, we find with $\mathcal{E}_M(t)=\int E_M\,\mathrm{d}k\propto t^{-(\beta+1)q}$ the line $p=2(1-q)$, which is also known as the self-similarity line [6, 32]. With $q=4/9$, we thus obtain $p=10/9$. This is all completely analogous to the MHD case with zero magnetic helicity; see also Table 2 of Ref. [31].[34] Thus, the cancelation of finite magnetic helicity by fermion chirality with $\mathcal{H}_M(t)=-2\mu_5(t)/\lambda\neq0$ has the same effect as that of zero magnetic helicity.

To understand the decay of magnetic helicity density in the present simulations, it is important to remember that the real space realizability condition of magnetic helicity [35] is always valid and implies $|\mathcal{H}_M|\le2\mathcal{E}_M\xi_M$. Assuming the inequality to be saturated, we find the scaling $|\mathcal{H}_M|\propto|\mu_5|\propto t^{-r}$ with $r=p-q=2/3$. This is well obeyed, as is shown in Figure 3(a). In Figure 3(b), we also show that $2\mathcal{E}_M\xi_M/\mathcal{H}_M\approx1$ at early times and about 1.1 at late times. Thus, we see that it is fairly constant, confirming therefore the validity of our underlying assumption. On top of this evolution of the chiral asymmetry, the growth rate of the chiral plasma instability, $\gamma_5\propto\mu_5^2\propto t^{-4/3}$, decays more rapidly than t^{-1}, which causes it to grow less efficiently so as not to spoil the scaling properties of the system.

To characterize the scaling expected from the conservation of the adapted Hosking integral further, we plot in Figure 4 the pq diagram of the instantaneous scaling exponents $p(t)=-\mathrm{d}\ln\mathcal{E}_M/\mathrm{d}\ln t$ versus $q(t)=\mathrm{d}\ln\xi_M/\mathrm{d}\ln t$. The solution converges to a point that is close to the crossing point between the $\beta=3/2$ line and the scale-invariance line $p=2(1-q)$. The approach to the point $(p,q)=(10/9,4/9)$ does not occur predominantly along the $\beta=3/2$ line, as in nonhelical standard MHD, but is now closer to the $r=2/3$ line, where $p=q+r$. In the unbalanced case, where the net chirality is non-vanishing, however, the decay is solely governed by $\langle h_{\rm tot}\rangle=$ const [21].

In conclusion, we have presented evidence that, in the balanced case of zero total chirality, the Hosking integral, when adapted to include the chiral chemical potential, is approximately conserved around the characteristic scale. This implies decay properties for magnetic energy and correlation length that are unchanged rela-

tive to nonhelical MHD, but here with $\mathcal{H}_{\rm M}+2\mu_5/\lambda=0$ (instead of $\mathcal{H}_{\rm M}=0$). This yields the novel scaling $|\mathcal{H}_{\rm M}|\propto|\mu_5|\propto t^{-2/3}$, along with the familiar scalings $\mathcal{E}_{\rm M}\propto t^{-10/9}$ and $\xi_{\rm M}\propto t^{4/9}$ that also apply to the case with $\mathcal{H}_{\rm M}=0$. These scalings have consequences for understanding the properties of the chiral magnetic effect in the early universe [13, 18–20, 36] and young neutron stars [37, 38].

We thank Valerie Domcke and Kai Schmitz for useful comments on the manuscript and Kyohei Mukaida for fruitful discussions. Support through the grant 2019-04234 from the Swedish Research Council (Vetenskapsrådet) (AB), Grant-in-Aid for Scientific Research Nos. (C) JP19K03842 from the JSPS KAKENHI (KK), and the grant 185863 from the Swiss National Science Foundation (JS) are gratefully acknowledged. We acknowledge the allocation of computing resources provided by the Swedish National Infrastructure for Computing (SNIC) at the PDC Center for High Performance Computing Stockholm and Linköping.

[1] L. Woltjer, "A Theorem on Force-Free Magnetic Fields," Proc. Nat. Acad. Sci. **44**, 489–491 (1958).
[2] J. B. Taylor, "Relaxation of Toroidal Plasma and Generation of Reverse Magnetic Fields," Phys. Rev. Lett. **33**, 1139–1141 (1974).
[3] A. Brandenburg and K. Subramanian, "Astrophysical magnetic fields and nonlinear dynamo theory," Phys. Rep. **417**, 1–209 (2005), astro-ph/0405052.
[4] David N. Hosking and Alexander A. Schekochihin, "Reconnection-Controlled Decay of Magnetohydrodynamic Turbulence and the Role of Invariants," Phys. Rev. X **11**, 041005 (2021), arXiv:2012.01393 [physics.flu-dyn].
[5] Alexander A. Schekochihin, "MHD turbulence: a biased review," J. Plasma Phys. **88**, 155880501 (2022).
[6] Hongzhe Zhou, Ramkishor Sharma, and Axel Brandenburg, "Scaling of the Hosking integral in decaying magnetically dominated turbulence," J. Plasma Phys. **88**, 905880602 (2022), arXiv:2206.07513 [physics.plasm-ph].
[7] Alexey Boyarsky, Jürg Fröhlich, and Oleg Ruchayskiy, "Self-Consistent Evolution of Magnetic Fields and Chiral Asymmetry in the Early Universe," Phys. Rev. Lett. **108**, 031301 (2012), arXiv:1109.3350 [astro-ph.CO].
[8] Igor Rogachevskii, Oleg Ruchayskiy, Alexey Boyarsky, Jürg Fröhlich, Nathan Kleeorin, Axel Brandenburg, and Jennifer Schober, "Laminar and Turbulent Dynamos in Chiral Magnetohydrodynamics. I. Theory," Astrophys. J. **846**, 153 (2017), arXiv:1705.00378 [physics.plasm-ph].
[9] Stephen L. Adler, "Axial vector vertex in spinor electrodynamics," Phys. Rev. **177**, 2426–2438 (1969).
[10] J. S. Bell and R. Jackiw, "A PCAC puzzle: $\pi^0\to\gamma\gamma$ in the σ model," Nuovo Cim. A **60**, 47–61 (1969).
[11] M. Joyce and M. Shaposhnikov, "Primordial magnetic fields, right electrons, and the abelian anomaly," Phys. Rev. Lett. **79**, 1193–1196 (1997).
[12] Yukinao Akamatsu and Naoki Yamamoto, "Chiral Plasma Instabilities," Phys. Rev. Lett. **111**, 052002 (2013), arXiv:1302.2125 [nucl-th].
[13] Kohei Kamada, "Return of grand unified theory baryogenesis: Source of helical hypermagnetic fields for the baryon asymmetry of the universe," Phys. Rev. D **97**, 103506 (2018), arXiv:1802.03055 [hep-ph].
[14] Valerie Domcke, Kohei Kamada, Kyohei Mukaida, Kai Schmitz, and Masaki Yamada, "A new constraint on primordial lepton flavour asymmetries," arXiv e-prints , arXiv:2208.03237 (2022), arXiv:2208.03237 [hep-ph].
[15] Raymond T. Co, Valerie Domcke, and Keisuke Harigaya, "Baryogenesis from Decaying Magnetic Helicity in Axiogenesis," arXiv e-prints , arXiv:2211.12517 (2022), arXiv:2211.12517 [hep-ph].
[16] Yuji Hirono, Dmitri E. Kharzeev, and Yi Yin, "Self-similar inverse cascade of magnetic helicity driven by the chiral anomaly," Phys. Rev. D **92**, 125031 (2015), arXiv:1509.07790 [hep-th].
[17] Jennifer Schober, Tomohiro Fujita, and Ruth Durrer, "Generation of chiral asymmetry via helical magnetic fields," Phys. Rev. D **101**, 103028 (2020), arXiv:2002.09501 [physics.plasm-ph].
[18] Valerie Domcke and Kyohei Mukaida, "Gauge field and fermion production during axion inflation," J. Cosmol. Astropart. Phys. **2018**, 020–020 (2018).
[19] Valerie Domcke, Benedict von Harling, Enrico Morgante, and Kyohei Mukaida, "Baryogenesis from axion inflation," J. Cosmol. Astropart. Phys. **2019**, 032 (2019), arXiv:1905.13318 [hep-ph].
[20] Valerie Domcke, Kohei Kamada, Kyohei Mukaida, Kai Schmitz, and Masaki Yamada, "Wash-in leptogenesis after axion inflation," J. High. Energy Phys. **01**, 053 (2023), arXiv:2210.06412 [hep-ph].
[21] See the Supplemental Material on `http://norlx65.nordita.org/~brandenb/projects/DecayWithChiral/` for comparisons of the decay law with vanishing and nonvanishing total chirality and comparisons with simulations where spin flipping is included.
[22] Kohei Kamada, Naoki Yamamoto, and Di-Lun Yang, "Chiral effects in astrophysics and cosmology," Prog. Part. Nucl. Phys. **129**, 104016 (2023), arXiv:2207.09184 [astro-ph.CO].
[23] Axel Brandenburg, Jennifer Schober, Igor Rogachevskii, Tina Kahniashvili, Alexey Boyarsky, Jürg Fröhlich, Oleg Ruchayskiy, and Nathan Kleeorin, "The Turbulent Chiral Magnetic Cascade in the Early Universe," Astrophys. J. **845**, L21 (2017).
[24] Axel Brandenburg, Yutong He, Tina Kahniashvili, Matthias Rheinhardt, and Jennifer Schober, "Relic Gravitational Waves from the Chiral Magnetic Effect," Astrophys. J. **911**, 110 (2021), arXiv:2101.08178 [astro-ph.CO].
[25] Axel Brandenburg, Tina Kahniashvili, Sayan Mandal, Alberto Roper Pol, Alexander G. Tevzadze, and Tanmay Vachaspati, "Evolution of hydromagnetic turbulence from the electroweak phase transition," Phys. Rev. D **96**, 123528 (2017).

[26] Ruth Durrer and Chiara Caprini, "Primordial magnetic fields and causality," J. Cosmol. Astropart. Phys. **2003**, 010 (2003), arXiv:astro-ph/0305059 [astro-ph].

[27] Pencil Code Collaboration, Axel Brandenburg, Anders Johansen, Philippe Bourdin, Wolfgang Dobler, Wladimir Lyra, Matthias Rheinhardt, Sven Bingert, Nils Haugen, Antony Mee, Frederick Gent, Natalia Babkovskaia, Chao-Chin Yang, Tobias Heinemann, Boris Dintrans, Dhrubaditya Mitra, Simon Candelaresi, Jörn Warnecke, Petri Käpylä, Andreas Schreiber, Piyali Chatterjee, Maarit Käpylä, Xiang-Yu Li, Jonas Krüger, Jørgen Aarnes, Graeme Sarson, Jeffrey Oishi, Jennifer Schober, Raphaël Plasson, Christer Sandin, Ewa Karchniwy, Luiz Rodrigues, Alexander Hubbard, Gustavo Guerrero, Andrew Snodin, Illa Losada, Johannes Pekkilä, and Chengeng Qian, "The Pencil Code, a modular MPI code for partial differential equations and particles: multipurpose and multiuser-maintained," J. Open Source Softw. **6**, 2807 (2021).

[28] Jennifer Schober, Igor Rogachevskii, Axel Brandenburg, Alexey Boyarsky, Jürg Fröhlich, Oleg Ruchayskiy, and Nathan Kleeorin, "Laminar and Turbulent Dynamos in Chiral Magnetohydrodynamics. II. Simulations," Astrophys. J. **858**, 124 (2018).

[29] J. Schober, A. Brandenburg, and I. Rogachevskii, "Chiral fermion asymmetry in high-energy plasma simulations," Geophys. Astrophys. Fluid Dynam. **114**, 106–129 (2020).

[30] See the Supplemental Material on `http://norlx65.nordita.org/~brandenb/projects/DecayWithChiral/` for plots showing the effect of the chiral plasma instability for different total chiralities and for comparisons with other weight functions.

[31] Axel Brandenburg, "Hosking integral in nonhelical Hall cascade," J. Plasma Phys., in press (2022), arXiv:2211.14197 [physics.plasm-ph].

[32] A. Brandenburg and T. Kahniashvili, "Classes of Hydrodynamic and Magnetohydrodynamic Turbulent Decay," Phys. Rev. Lett. **118**, 055102 (2017), arXiv:1607.01360 [physics.flu-dyn].

[33] P. Olesen, "Inverse cascades and primordial magnetic fields," Phys. Lett. B **398**, 321–325 (1997), arXiv:astro-ph/9610154 [astro-ph].

[34] See also the discussion in Ref. [39] for weak magnetic field with zero magnetic helicity, where selfsimilarity is not assumed.

[35] T. Kahniashvili, A. G. Tevzadze, A. Brandenburg, and A. Neronov, "Evolution of primordial magnetic fields from phase transitions," Phys. Rev. D **87**, 083007 (2013), arXiv:1212.0596 [astro-ph.CO].

[36] L. Del Zanna and N. Bucciantini, "Covariant and 3 + 1 equations for dynamo-chiral general relativistic magnetohydrodynamics," Mon. Not. R. Astron. Soc. **479**, 657–666 (2018), arXiv:1806.07114 [astro-ph.HE].

[37] Youhei Masada, Kei Kotake, Tomoya Takiwaki, and Naoki Yamamoto, "Chiral magnetohydrodynamic turbulence in core-collapse supernovae," Phys. Rev. D **98**, 083018 (2018), arXiv:1805.10419 [astro-ph.HE].

[38] Maxim Dvornikov, V. B. Semikoz, and D. D. Sokoloff, "Generation of strong magnetic fields in a nascent neutron star accounting for the chiral magnetic effect," Phys. Rev. D **101**, 083009 (2020), arXiv:2001.08139 [astro-ph.HE].

[39] Fumio Uchida, Motoko Fujiwara, Kohei Kamada, and Jun'ichi Yokoyama, "New description of the scaling evolution of the cosmological magneto-hydrodynamic system," arXiv e-prints , arXiv:2212.14355 (2022), arXiv:2212.14355 [astro-ph.CO].